

Article

Evaluation of Nano Zero-Valent Iron (nZVI) Activity in Solution and Immobilized in Hydrophilic PVDF Membrane for Drimaren Red X-6BN and Bisphenol-a Removal in Water

Larissa L. S. Silva ^{1,*} , Júlio A. Caldara ¹, Ana Maria Rocco ¹, Cristiano P. Borges ² and Fabiana V. Fonseca ^{1,*} 

¹ School of Chemistry, Federal University of Rio de Janeiro, Rio de Janeiro 20211, Brazil; jcaldara32@gmail.com (J.A.C.); amrocco@eq.ufrj.br (A.M.R.)

² Chemical Engineering Program, COPPE, Federal University of Rio de Janeiro, Rio de Janeiro 20011, Brazil; cristiano@peq.coppe.ufrj.br

* Correspondence: larissaloureiros@hotmail.com (L.L.S.S.); fabiana@eq.ufrj.br (F.V.F.); Tel.: +55-21-3938-8347 (L.L.S.S.); +55-21-3938-7590 (F.V.F.)

Received: 5 November 2019; Accepted: 26 November 2019; Published: 2 December 2019



Abstract: Fenton reactions that involve nano zero-valent iron (nZVI) have shown high promise in the removal of organic pollutants. In this work, nZVI stabilized with carboxymethyl cellulose (CMC) was evaluated for drimaren red X-6BN (DRX-6BN, 10 mg/L) and bisphenol-a (BPA, 800 mg/L) removal. Oxidation reactions were conducted for removal of both compounds by varying nZVI/CMC concentration (0.01–5 g/L), hydrogen peroxide (H₂O₂, 0.01–0.1 g/L), and pH (3–9). DRX-6BN degradation rate was the highest (kinetic constant (k_{obs}) = 4.622 h⁻¹) when working at pH 3 and 3 g/L of nZVI/CMC. Increasing H₂O₂ concentration could not improve the reaction. For BPA, all the conditions tested showed removals of more than 96% with 0.02 g/L of H₂O₂. This result was compared with the activity of nZVI loaded in hydrophilic PVDF (Polyvinylidene fluoride) membranes by polyacrylic acid (PAA) to entrap nanoparticles to the membrane surface. As expected, the attachment of nZVI onto the membranes diminished nanoparticles' activity; however, it is important to highlight the need for preparing a stable catalytic membrane, which could enhance pollutant removal of microfiltration membranes' systems. This was confirmed by the percentage of iron leaching from functionalized membranes, where a higher concentration of iron in the bulk solution leads to enhancement on BPA removal. Issues with BPA diffusion resistance inside the pores were overcome by conducting the nZVI/PAA/PVDF membranes in the cross-flow system, reaching 40% of BPA removal after 3 h of permeation.

Keywords: nZVI; PVDF membranes; Drimaren red X-6BN; Bisphenol-a; polyacrylic acid

1. Introduction

Fenton reactions that involve nano zero-valent iron (nZVI) as a catalyst has shown high promise in the degradation of various recalcitrant contaminants (such as pharmaceuticals, personal care products, and pesticides) in water by achieving their mineralization via •OH radical generation [1–3]. Due to its characteristic as a strong reducing agent, nZVI has been also applied for the dechlorination of trichloroethylene and polychlorinated biphenyls, as well as decolorization of dyes (reactive black 5 and reactive red 198) and removal of antibiotics (tetracycline) [4–7].

However, due to the fast aggregation of ZVI nanoparticles, which diminishes their activity quickly, the surface modification for their stabilization applying carboxymethyl cellulose (CMC), polyelectrolyte

multilayers, smectite, polyacrylic acid (PAA), poly(ethylene glycol) (PEG), or poly(methylmethacrylate) has been widely investigated [6,8,9]. CMC polymer features highly effective on nZVI stability, leading to nanoparticles with an average size of 10–100 nm [10,11] and maintaining or even increasing its activity up to 40 times on triazine removal, for example [12].

Another technique to avoid nanoparticles aggregation is their immobilization in different porous media, such as silica, activated carbon, resin, zeolite, and membranes [3,6,8,10,13,14]. In membranes, for example, nZVI can improve the permeation process by lowering the deposition of contaminants in the membrane surface as well as increasing its hydrophilicity [13]. This composite material has been synthesized by different techniques (i.e., sol-gel process, in situ chemical reduction, and in situ polymer action) [15], but the ion exchange route shows high promise on increasing permeability (e.g., 116% of improvement with 3% of AlCl₃ loaded in polyvinylidene fluoride-PVDF-membrane) and hydrophilicity (contact angle diminished from 73.6° to 52.3° in ZrO₂/PES membrane) [16,17]. Moreover, nZVI composite membranes synthesized by the ion exchange route show high stability of the nanoparticles owing to the strong binding between the chelant agent active sites (i.e., PAA and PEG) and the nZVI [18–21].

Because of the high promise on a stable material with a minimum loss of nanoparticles, these nZVI composite membranes have been used for degradation of metronidazole, metoprolol, trichloroethylene, and methylene blue as well as removal of metals, such as copper, nickel, chromium, bromate, and cadmium, in water [18–23]. The described organic compounds are removed mostly by the reduction pathway [18–21], leaving a lack of information about the oxidation of the target organic contaminants by the nZVI composite membranes.

This work proposes an investigation of the efficiency of the nZVI composite membrane on bisphenol-A (BPA) removal through the oxidation pathway by applying H₂O₂ as an oxidant. Also, experiments with nZVI in solution, stabilized by CMC polymer, were conducted to evaluate drimaren red X-6BN (DRX-6BN) and BPA removal and the results were compared with the efficiency of nZVI composite membranes.

2. Materials and Methods

2.1. Chemicals and Reagents

The reagents iron (II) chloride tetrahydrate (FeCl₂·4H₂O, ≥99.0%), sodium borohydride (NaBH₄, ≥98.0%), acrylic acid (AA, 99.0%), potassium persulfate (K₂S₂O₈, ≥99.0%), ethylene glycol (EG, 99.5%), BPA (98%), CMC (90,000 Daltons), and polyvinylpyrrolidone (PVP) were purchased from Sigma-Aldrich. Ethanol (anhydrous, ≥99.5%), N-Methyl-2-pyrrolidone (NMP, synthesis), and hexane (mixture of isomers) were from Isosfar. PVDF (Kynar[®] 740) was acquired from Arkema. Hydrogen peroxide (H₂O₂, 50% v/v, 200 VLS) and acetone (99.5%) were purchased from Sumatex[©] and Qhemis, respectively.

2.2. Synthesis of Nano Zero-Valent Iron (nZVI)/Carboxymethyl Cellulose (CMC)

nZVI preparation was adapted from previous work [10]. Briefly, 0.5 g of CMC was dissolved in 100 mL of deoxygenated ultra-pure water and 20 mL of FeCl₂ solution (25.35 g/L) were added, followed by sonication (150 RMS) for 30 min under N₂ purge. 50 mL of NaBH₄ solution (7.57 g/L) were added dropwise to the solution/sonication/N₂ system and sonicated for 2 h more. At the end of the reduction reaction, nZVI were centrifuged (7000 rpm) and washed twice with acetone to remove unreacted chemicals. The nanoparticles were then dried under N₂ at 90 °C and stored under N₂. Right before using them for degradation experiments, nZVI were resuspended with water, in specific concentrations, for 5 min under sonication and N₂. The efficiency of nZVI synthesis provided 1.6 g nZVI/mL of FeCl₂ solution.

2.3. nZVI/PAA/PVDF Membrane Preparation

Hydrophilic PVDF flat-sheet membranes were used as a chemical- and thermal-resistant porous material for nZVI loading [10,13,24]. These membranes were prepared by phase inversion with the immersion precipitation technique with 14% of PVDF and 7.5% of PVP in NMP. PVP was used as a hydrophilic additive to improve nanoparticles' loading [25]. After dissolving the polymers, the polymeric solution was kept without stirring for 4 h to remove bubbles and then was cast on glass plates (20 × 25 cm) with a 150 µm thickness knife. 7 min of environment air exposure (65% humidity) and water/NMP:70/30 coagulation bath were conducted to enhance pore formation on the membrane. The membranes were then immersed in ultra-pure water for 2 days, with water replacement twice per day, followed by immersion in ethanol and hexane baths. Then, the hydrophilic PVDF membranes were left to dry at room temperature. The as-prepared membranes showed an average pore size of 0.6 µm.

nZVI immobilization in the hydrophilic PVDF membranes was achieved by in situ polymerization of AA at the same time as the crosslink of PAA with PEG. The methodology of polymerization/crosslink of PAA was adapted from previous work [10,24,26,27], which was based on dissolving the initiator ($K_2S_2O_8$) in deoxygenated ultra-pure water, followed by adding AA monomer and the crosslinking agent (EG). Different concentrations of the reagents were evaluated for the hydrophilic PVDF membrane functionalization, as described in Table 1. Hydrophilic PVDF membranes were immersed in the polymerization solution for 5 min and at the best relation of iron loading/leaching, 10 mL of the polymerization solution was filtrated (Millipore® filtration system) through the membrane. This last step was tested to ensure that all pores of the hydrophilic PVDF membrane were functionalized with PAA.

Table 1. Concentration of AA, EG, $K_2S_2O_8$ and H_2O in polymerization solution and contact time with hydrophilic PVDF membrane for functionalization with PAA.

Membrane	AA (wt. %)	EG (mol % of AA)	$K_2S_2O_8$ (wt. %)	Contact Time (min)
20% AA	20	1.0	1.0	5
30% AA	30	1.0	1.0	5
30% AA *	30	1.0	1.0	Filtration (10 mL) ¹
40% AA	40	1.0	1.0	5

¹ Membrane contact time in AA solution was replaced by filtration in dead-end mode: mean permeate flow rate of 0.12 L/h and membrane contact time with AA solution of 5 min. EG (ethylene glycol); AA (acrylic acid); PVDF (Polyvinylidene fluoride); PAA (Polyacrylic acid).

Right after the contact with polymerization solution, AA/PVDF membranes were sandwiched between two glass plates and put in a modified oven with N_2 purge to avoid the presence of oxygen that could lead to secondary reactions and constrain the linkage of PAA chains [10,24,26,27]. The oven was set at 90 °C for 4 h of reaction. The glass plates were then cooled down to room temperature and detached using ethanol.

PAA/PVDF membranes were loaded with nZVI by the ion exchange technique [10,24]. The membranes were immersed in 200 mL of NaCl solution (4 g/L, pH 9.5–10.0—NaOH 0.5 mM) for 24 h, followed by washing with ultra-pure water until pH 7.0 ± 0.5. Na^+ /PAA/PVDF membranes were then put in contact with 200 mL of $FeCl_2$ solution (1 g/L, pH 5.0–5.5) for 4 h under N_2 purge. This step is based on the facilitated ion exchange between Na^+ and $Fe^{2+/3+}$ on the active sites of PAA ($-COO^-$) [10,24]. nZVI/PAA/PVDF membranes were acquired with the contact of these membranes with 50 mL of $NaBH_4$ (40 g/L). All the membranes (17.3 cm²) were stored in ethanol for the following tests.

2.4. nZVI/CMC and nZVI/PAA/PVDF Membrane Characterization

A MiniFlex II-Rigaku diffractometer X-ray diffraction (XRD) was used to determinate the crystalline structure of the nanoparticles. Size distribution and zeta potential of nZVI/CMC were verified by Zetasizer Nano S-Malvern and Zeta Plus-BTC (BrookHaven Instruments Corporation), respectively.

FEI (Field Electron and Ion) Company Quanta 200, EDT (Everhart-Thornley detector), 90–100 μ A, a scanning electron microscopy (SEM) equipment, were used for investigation of membrane surface morphology and the cross-section, as well as the nZVI/CMC. For the cross-section images, the membranes were immersed in liquid N_2 and fragmented into two pieces for proper view. The ImageJ program was used as a tool to obtain the nanoparticles' size and distribution as well as the average pore size from PVDF membranes. PAA polymerization and cross-link were verified by Fourier transform infrared spectroscopy (FTIR), FTIR 3100-Excalibur Series, Varian. The contact angle of the membranes was measured by Dataphysics, German, OCA15 (Optical contact angle measuring and contour analysis systems) equipment.

Nanoparticles' concentration per area of membrane sheet was calculated by the diminished iron concentration inside the $FeCl_2$ solution after the ion exchange step ($Na^+ \rightarrow Fe^{2+/3+}$) (validated by Gui et al. [10]). Total iron was measured by the Hach[®] kit (FerroVer[®] Iron reagent).

2.5. nZVI/CMC Activity for Drimaren Red X-6BN (DRX-6BN) and Bisphenol-a (BPA) Removal

To investigate nZVI/CMC efficiency, two organic recalcitrant compounds were evaluated: DRX-6BN and BPA. The first is a complex organic molecule holding azo groups ($-N=N-$) in its structure, and the latter is known as an endocrine disruptive which has two phenol groups [28,29].

The experiments for the target compounds' degradation were conducted in tubes holding 40 mL of total reaction in a shaker at 150 rpm and 25 $^{\circ}C$. Samples were taken in specific times (0–4 h) and filtrated using a syringe filter (cellulose acetate, 0.45 μ m). The concentration of both compounds was measured by a Shimadzu—UV1800 spectrophotometer with 276 and 511 nm wavelength for BPA and DRX-6BN, respectively. Different concentrations of nZVI/CMC and H_2O_2 , as well as a range of pH was tested for DRX-6BN and BPA removal (Table 2).

Table 2. Experiments conducted for drimaren red X-6BN (DRX-6BN) and bisphenol-a (BPA) removal according to pH, nZVI/CMC, and H_2O_2 concentration.

Compound Initial Concentration	nZVI/CMC (g/L)	H_2O_2 (g/L)	pH	
(DRX-6BN) ₀ = 10 mg/L	0.1	0.1	5.0	
	0.5	0.1	5.0	
	1	0.1	5.0	
	2	0.1	5.0	
	3	0.01	3.0	
	3	0.05	3.0	
	3	0.1	3.0	
	3	0.1	5.0	
	3	0.1	7.0	
	3	0.1	9.0	
	5	0.1	5.0	
	(BPA) ₀ = 800 mg/L	0.1	0.02	3.0
		0.5	0.02	3.0
1.0		0.02	3.0	

2.6. nZVI/PAA/PVDF Membrane Activity for BPA Removal

nZVI/PAA/PVDF membranes were first tested in solution to evaluate the relation of the percentage of iron loading (i.e., according to different percentages of AA polymeric solution described in Table 1), BPA removal, and iron leaching. The membranes were immersed in a BPA solution (800 mg/L) with a

specific volume to reach a concentration of 0.1 g/L of nZVI for each membrane. H₂O₂ concentration was set at 0.02 g/L after promising results acquired from the nZVI/CMC tests. Although the tests with nZVI/CMC presented pH 3.0 as the best condition for the target compounds removal, the experiments with nZVI/PAA/PVDF membranes were carried out at pH 5.0 to avoid nanoparticles' detachment from PAA active sites, thus enhancing membrane lifetime. Samples were taken with 1 and 24 h, also filtered through a syringe filter.

The best condition of the above tests was used to fabricate the nZVI/PAA/PVDF membrane and to evaluate its activity in convective mode. The cross-flow membrane system with 12.6 cm² of active area cell, operated with recirculation of retentate and the Remco 3323-2F1-82B pump, was used for BPA (800 mg/L) removal. A pressure gauge (set at 1 bar) was installed in the concentrate, followed by a pressure regulator. The reservoir (1.5 L) received constant concentrate and permeate feeds. Samples of 5 mL were collected in specific times (0–3 h) from the permeate for analysis of BPA concentration. The flux was measured by the time that the permeate took to achieve a certain volume (i.e., the volume changed from 5 to 50 mL according to the flux and the membrane). Fenton reaction, driven by nZVI/PAA/PVDF membranes and H₂O₂ (0 and 20 mg/L) in the feed solution, was investigated at pH 5 to avoid nanoparticles' detachment from PAA active sites, thus enhancing membrane lifetime. PVDF membranes were also tested in order to verify the adsorption phenomena of BPA into the membranes.

3. Results and Discussion

3.1. Nanoparticles' Characterization

nZVI/CMC nanoparticles' formation was confirmed by the analysis shown in Figure 1. Size distribution (Figure 1A) revealed nZVI/CMC particles with two major peaks at the size of 75.6 nm (width: 32.8 nm) and 417.7 nm (width: 187.1 nm), as well as the z-average diameter of 109.0 nm (Polydispersity Index-PDI: 0.483). As CMC polymer acts as a stabilizer to avoid nanoparticles' aggregation by implying negative charges in the upper layer [3,9,10], its presence as a nonreacted polymer in the sample solution could generate the double peak. This was confirmed (Figure 1B) by the peak at 624.6 nm (width: 102.0 nm) and z-average diameter of 1067 nm (PDI: 0.633) for just CMC particles in the solution. The SEM image (Figure 1E) of nZVI/CMC suggests nanoparticles with an average size of 60 nm. Applying the same technique, Gui et al. achieved iron oxides nanoparticles with 76 nm of diameter due to agglomeration effects [10]. XRD (Figure 1C) also confirmed the reduction of Fe^{2+/3+} to Fe⁰ (α -Fe = 44.7⁰, 65.2⁰, and 82.4⁰) as well as the presence of Fe₂O₄ (35.6⁰, 56.9⁰, and 62.3⁰). The surface of the nanoparticles were revealed to be negatively charged at pH \geq 3.0 (Figure 1D), which can be associated with the presence of CMC (dissociation constant-pK_a = 4.0), presenting carbonyl groups (-COO⁻) dissociated [10].

3.2. BPA and Dye Removal by nZVI in Solution

nZVI has been widely studied for the oxidation of pharmaceuticals and herbicides because of its capability of reducing dissolved oxygen (O₂) and producing H₂O₂, which reacts with the iron leached from the material to generate hydroxyl radicals (\bullet OH) [3,8,30]. Generally, this approach was followed by deactivation of the catalyst in a short period, diminishing the efficiency of the system. Thus, to increase the kinetics of DRX-6BN removal by nZVI/CMC, the behavior of a fixed dose of H₂O₂ (0.1 g/L) at different nanoparticles' concentration was investigated in this work (Figure 2).

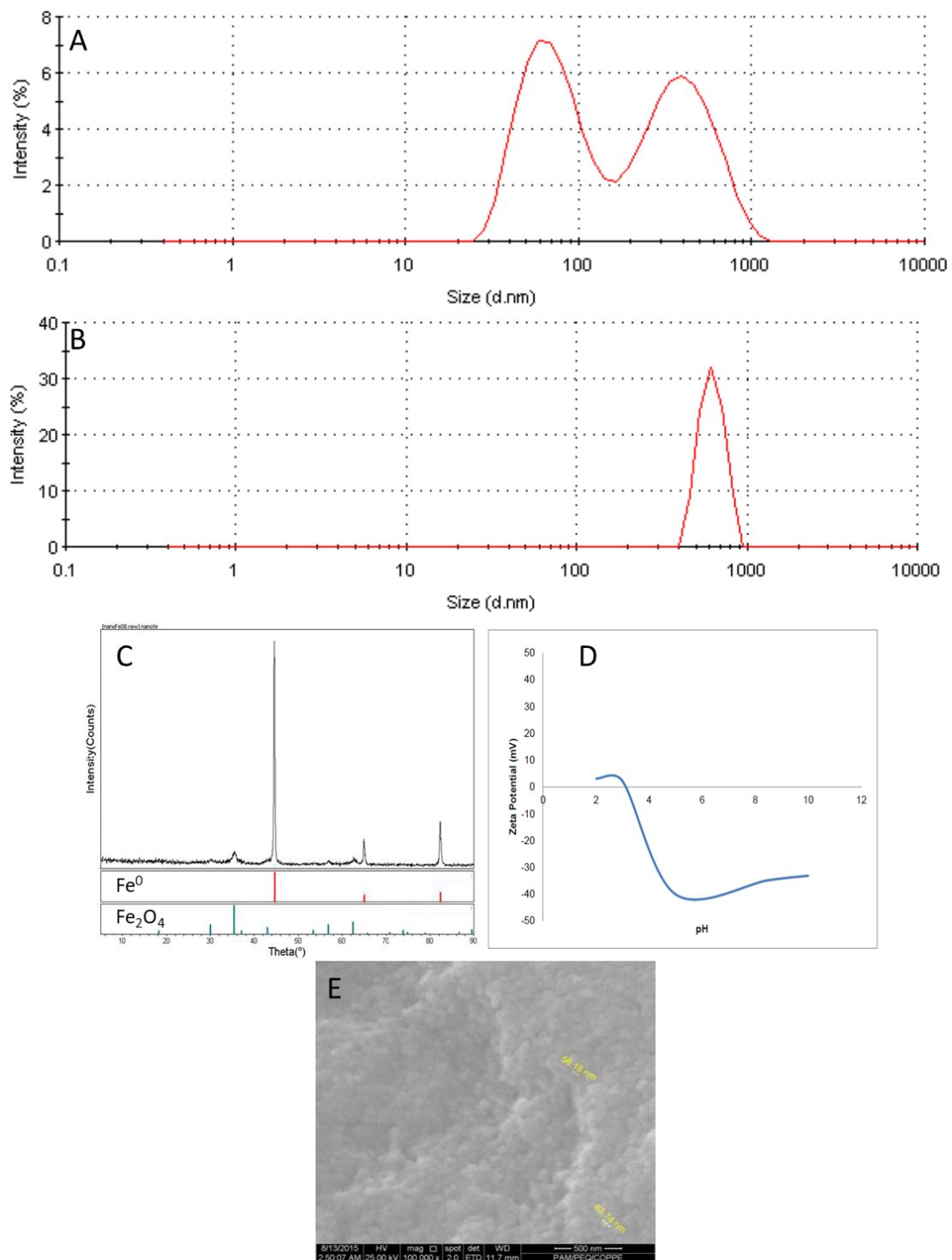


Figure 1. Nanoparticles' characterization: size distribution of nZVI/CMC (A) and CMC (B); X-ray diffraction (XRD) (C), zeta potential, (D) and scanning electron microscopy (SEM) image of nZVI/CMC (E).

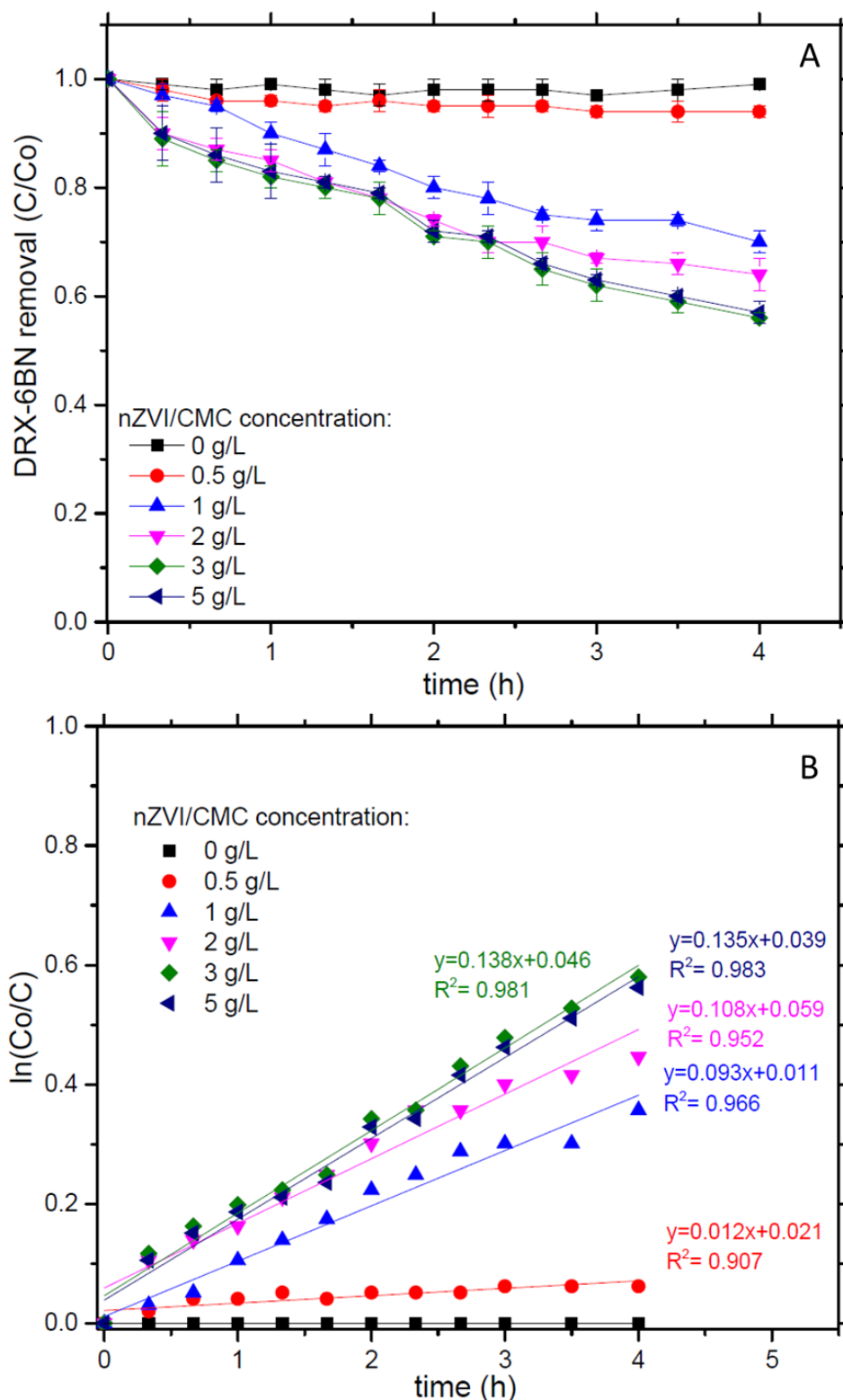


Figure 2. (A) DRX-6BN removal and (B) kinetics. Conditions: DRX-6BN₀ = 10 mg/L, nZVI/CMC = 0–5 g/L, H₂O₂ = 0.1 g/L and pH 5.0.

The results show that increasing nanoparticles' concentration from 0.5 to 1.0 g/L led to improvements on dye removal up to 36%, at 3 g/L reaching the best relation of nanoparticles/H₂O₂ with 44% of DRX-6BN removal within 4 h. A higher concentration of nZVI/CMC—5 g/L—requires more H₂O₂ available for •OH formation, as a result, DRX-6BN removal was similar to that achieved with

3 g/L of nanoparticles. Reaction kinetics were further investigated (Figure 2B), thus the data presented on Figure 2A were fitted to pseudo-first-order model according to Equation (1),

$$\ln \frac{C_0}{C} = k_{\text{obs}} \times t, \quad (1)$$

where C_0 and C is the initial ($t = t_0 = 0$) and final ($t = t_{0+i}$) concentration of DRX-6BN, k_{obs} is the rate constant of pseudo-first order (h^{-1}), and t is the reaction time (h).

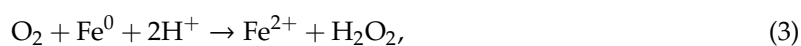
The kinetic removal of DRX-6BN was almost 8-fold higher when the nZVI/CMC concentration increased from 0.5 to 1.0 g/L (i.e., k_{obs} 0.012 and 0.093 h^{-1} , respectively). However, nanoparticles' concentration at 2 g/L had a slight augment in k_{obs} (0.108 h^{-1}) compared to 1.0 g/L of nZVI, increasing to 0.138 h^{-1} with 3 g/L. Thus, the concentration of nZVI/CMC at 3 g/L showed the best condition for further experiments, representing the least concentration of catalyst that gave the maximum removal response.

Fenton reactions show high effectiveness on organic contaminants' degradation [1,2,8,30]. This is a result of inducing the generation of $\bullet\text{OH}$ according to Equation (2),



where Fe^{2+} is converted to Fe^{3+} by reducing H_2O_2 [30].

According to Harada et al. [30], ZVI nanoparticles are capable to generate $\bullet\text{OH}$ radicals by the corrosion of Fe^{2+} from the nanoparticle surface [30]. H_2O_2 also generated by the oxygen presented in the solution (Equation (3)) will react with Fe^{2+} released to form $\bullet\text{OH}$ radicals (Equation (2)) [30,31]. Also, Fe^{2+} leaching can be seen by the reaction between nZVI and H_2O as in Equation (4) [31],



When this process occurs at $\text{pH} \geq 7$, OH^- ions are in abundance and react with iron ions in the solution to form hydroxides or oxygenized species (e.g., $\text{Fe}(\text{OH})_2$, $\text{Fe}(\text{OH})_3$, Fe_2O_3 , FeO , Fe_3O_4 , and FeOOH), decreasing the efficiency of radicals' generation [1,2,30]. Yet, the application of nZVI to these systems is suggested as a catalyst capable of inducing $\bullet\text{OH}$ formation in pH near to neutral by the corrosion of the nanoparticle surface, which is mediated by the presence of O_2 [3,8]. Furthermore, Harada et al. depict the behavior of nZVI and the gradual enhancement of $\bullet\text{OH}$ formation when the pH is decreased from 7 to 3 in oxygenated water [30].

To verify the role of pH on nZVI/CMC activity for organic compounds' removal, Figure 3A presents the degradation of XRD-6BN according to different pH values at 3 g/L of catalyst and 0.1 g/L of H_2O_2 . The results show that at basic pH (9 and 7), just a slight dye removal (30% in both conditions) was achieved, whereas at pH 3, XRD-6BN concentration dropped almost instantaneously (i.e., 78% in 5 min), reaching more than 99.9% of removal in 1 h of reaction. Kinetic constants were also calculated by Equation (1). In Figure 3B, the reaction with pH 3 shows k_{obs} equal to 4.513 h^{-1} , while for pH 7 and 9 it is 0.089 and 0.092 h^{-1} of k_{obs} . These results imply that the pH is still a variable that must be taken into consideration for reactions with nZVI/CMC. It is worthwhile to point out that works that had applied nZVI supported in other materials, such as resins, bentonite, and PVP, could reach dye removals more than 95% at pH higher than 5.6 [8]. In those cases, adsorption phenomena could be involved, enhancing the overall results.

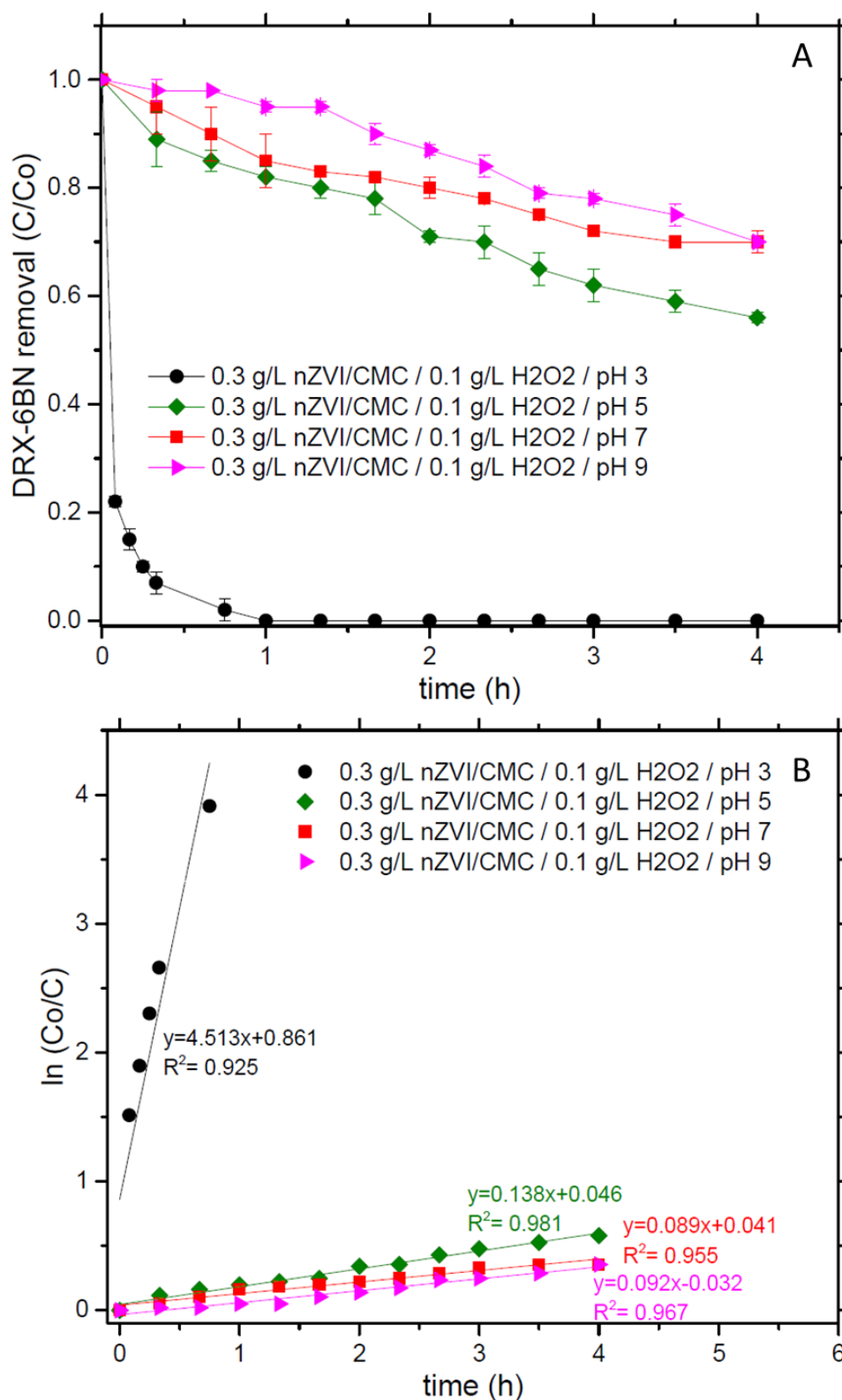


Figure 3. (A) DRX-6BN removal and (B) kinetics. Conditions: DRX-6BN₀ = 10 mg/L, nZVI/CMC = 3 g/L, H₂O₂ = 0.1 g/L, and pH 3–9.

To validate the oxidant concentration avoiding its excess, the H₂O₂ dose was varied from 0.01 to 0.1 g/L, with 3 g/L of nZVI/CMC at pH 3 (Figure 4). The results did not show any difference between

the conditions, reaching, at 20 min, 93% of XRD-6BN removal. Kinetic constants also remained the same ($k_{obs} \approx 4.6$).

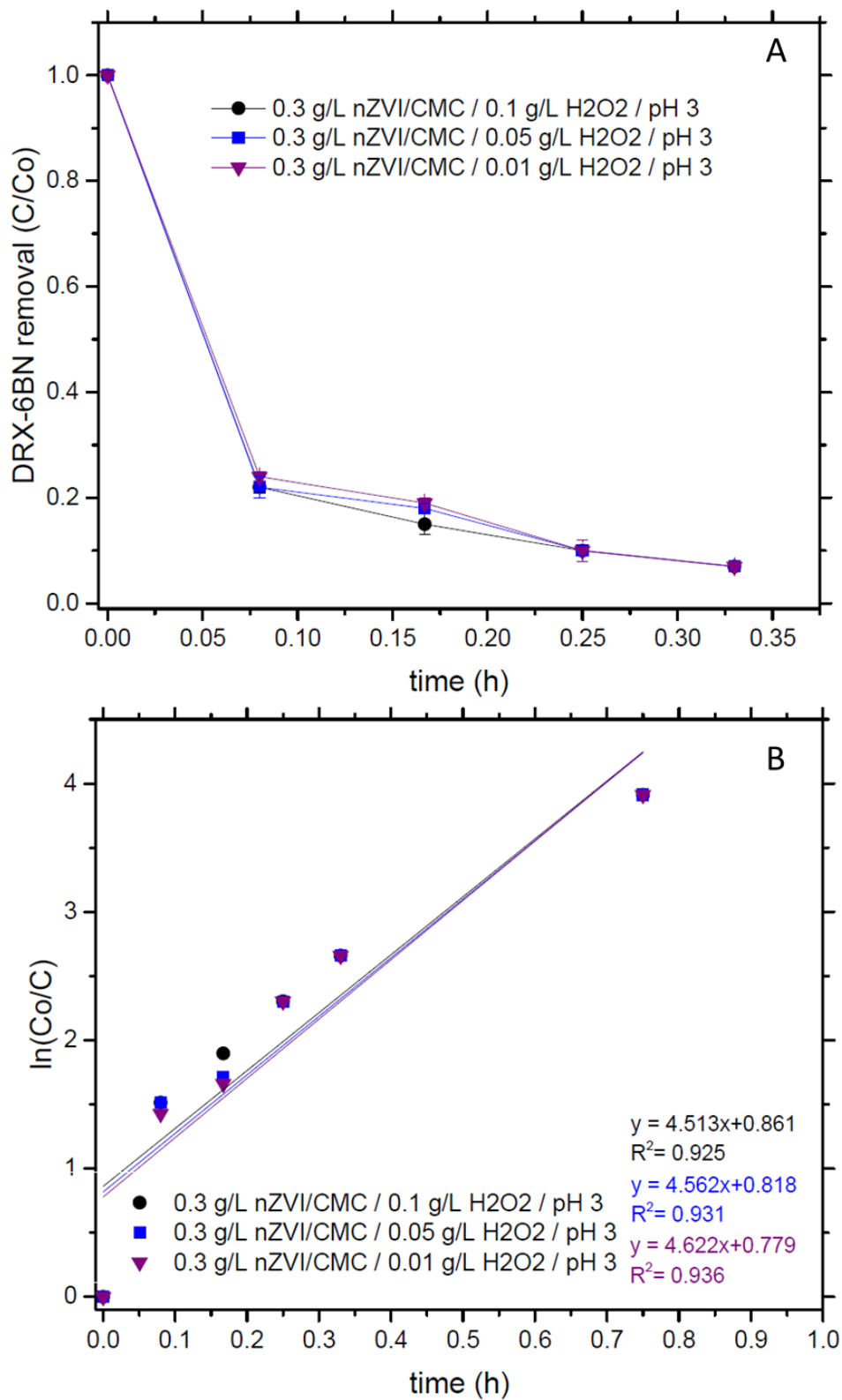


Figure 4. (A) DRX-6BN removal and (B) kinetics. Conditions: DRX-6BN₀ = 10 mg/L, nZVI/CMC = 3 g/L, H₂O₂ = 0.01–0.1 g/L, and pH 3.

The removal behavior of XRD-6BN by Fenton-like reactions with the nZVI/CMC catalyst worked as a probe to the following reactions with BPA. So, to investigate whether the nanoparticles are efficient on BPA removal for further experiments with nZVI impregnated on membranes, experiments were conducted varying nZVI/CMC concentration at a fixed H₂O₂ dose (0.02 g/L) and pH 3. High BPA concentration (800 mg/L) was selected to diminish adsorption phenomena effects on further tests with polymeric membranes. Table 3 shows the high efficiency of BPA removal by the nZVI/CMC/H₂O₂ system at pH 3. With 0.5 and 1.0 g/L of nZVI/CMC, the compound was not detected within 1 h of reaction. However, using 0.1 g/L of catalyst, the removal percentage decayed to 96%. This result served as a pre-concept for the experiments with nZVI impregnated onto membranes.

Table 3. BPA removal by different concentrations of nZVI at pH 3.0, 20 mg/L H₂O₂, and 1 h of reaction. BPA₀ = 800 mg/L.

nZVI/CMC (g/L)	BPA Removal (%)
0.1	96
0.5	100
1	100

3.3. PAA Functionalized PVDF Membranes and Correlation with nZVI Loading, Iron Leaching, and BPA Removal

Different degrees of PAA functionalization on PVDF membranes have been addressed by previous work [13]. Islam et al. correlated the mass gain of PAA/PVDF membranes to the AA content in polymerization solution and percentage of crosslink agent as well as the iron loading, reaching a specific condition (e.g., 20% wt. of AA and 1% mol of acrylamide) for the maximum of iron in the membranes [13]. However, a comprehensive mechanism on iron leaching according to the PAA functionalization degree and the effectiveness of these systems is still obscure for nZVI/PAA/PVDF membranes.

In order to enlighten the role of iron leaching from nZVI/PAA/PVDF membranes, Figure 5 depicts different percentages of it and the correlated BPA removal. The results with 1 h of reaction (Figure 5A) showed an augment on BPA removal according to dissolved iron in the bulk (i.e., 17.5%, 24.0%, 60.5%, and 98.5% of BPA removal with 0%, 0%, 3%, and 4% of iron leaching from the membrane, for the 30% AA*, 30% AA, 20% AA, and 40% AA membranes, respectively). Non-detected residuals of iron leachate could be involved in BPA removal for 30% AA prepared membranes. Adsorption phenomena are likely involved, representing 0.7% of BPA removal (i.e., experiment conducted at the same conditions but with PVDF membrane). Tests conducted with just BPA and BPA/H₂O₂ did not present any significant removal (<0.1%).

Longer reaction time (24 h) enhanced the overall BPA removal (Figure 5B), once iron leaching increased for almost all membranes (i.e., 37.2%, 51.5%, 82.2%, and 100% of BPA removal with 0%, 1%, 3%, and 16% of iron leaching, respectively). According to Equation (2), Fe²⁺ must be in the solution to generate •OH radicals for organic pollutant removal. The longer time was also favorable to blank reactions, where BPA volatilization and adsorption was 5.3% and 14.5%, respectively. This behavior suggests that adsorption phenomena achieved the equilibrium within 24 h and during this time, BPA is subjected to volatilization. Considering the membranes which did not present increases on iron leaching (i.e., 20% AA and 30% AA*), the longer time revealed the diffusion resistance as a parameter that must be considered, once the target compound needs to adsorb into the pore's material to be degraded by the oxidant species. These results confirm the decrease of nanoparticles' activity when they are impregnated on supporting materials [10].

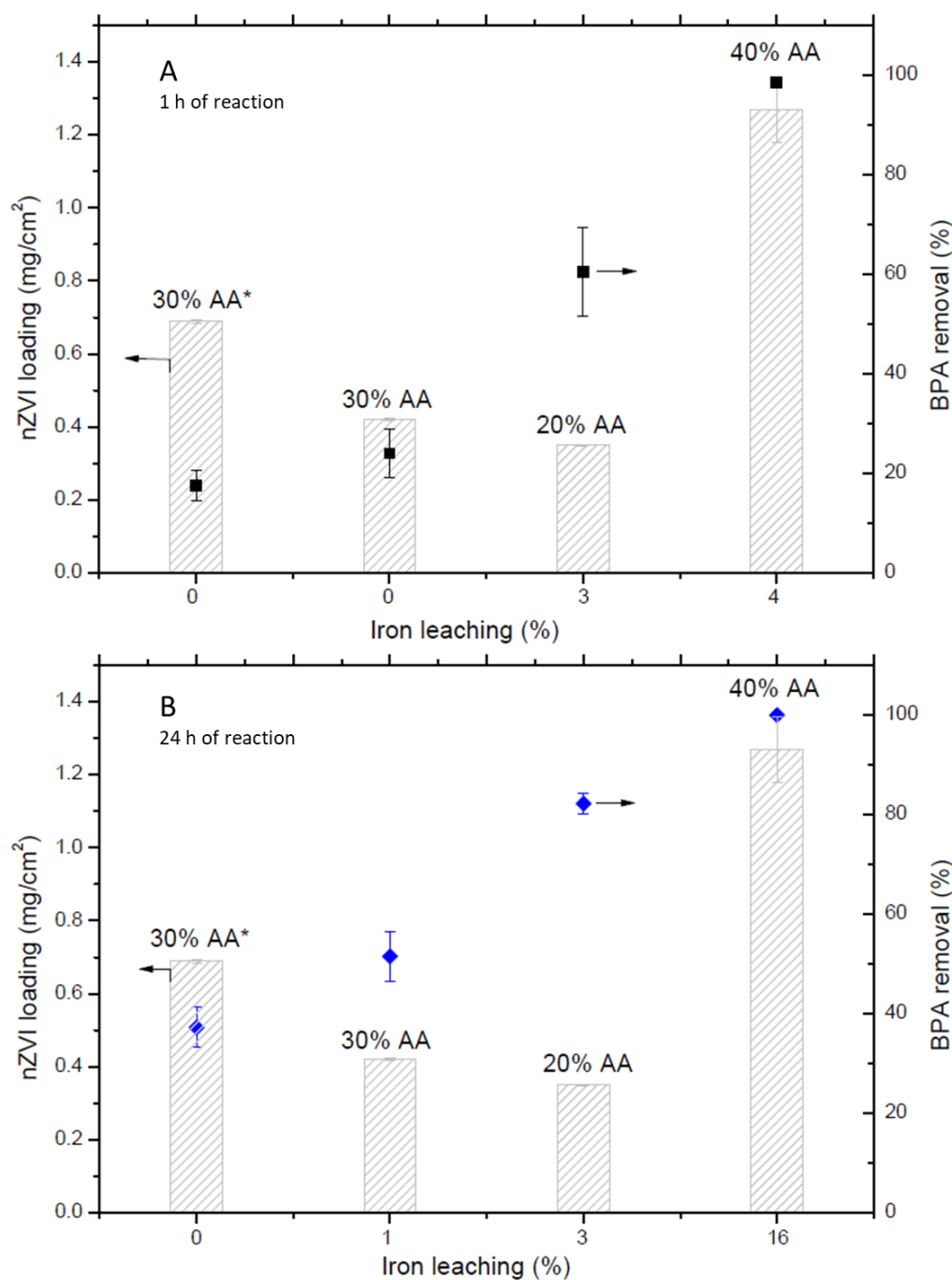


Figure 5. nZVI loading and BPA removal according to iron leaching from nZVI/PAA/PVDF membranes prepared with 20%, 30%, and 40% of AA. 30% AA* = nZVI/PAA/PVDF membrane prepared with filtration of AA polymeric solution. (A) 1 h and (B) 24 h of reaction at pH 5.0, 0.1 g/L nZVI (impregnated in the membrane), 20 mg/L H₂O₂, and (BPA)₀ = 800 mg/L.

Regarding the membranes which did not present detectable iron leaching after 1 h of reaction (membrane prepared with 30% of AA), improvements on PAA functionalization were performed to ensure that all membranes pores were filled. 10 mL of 30% AA polymeric solution was filtrated through the PVDF membrane (30% AA*). As a result, nanoparticles' loading increased (0.69 mg/cm²) compared to the membranes prepared with immersion in the AA polymeric solution (0.42 mg/cm², Figure 5). Membranes prepared with 20% AA leached 3% of its impregnated iron (0.35 mg/cm²) and the ones prepared with 40% showed an increase in iron leaching from 4% to 16% (reaction time of 1 and 24 h,

respectively). A specific combination of AA monomer and crosslink agent should be achieved in order to obtain the maximum deprotonated carboxyl groups for nanoparticles' loading [13]. At the same time, the crosslink must be sufficient to properly entrap nanoparticles in the polymer chain and avoid leaching effects. A higher ratio of crosslinker/AA can diminish the number of active sites available for nanoparticles' loading, once the same carboxyl groups will be responsible for both nanoparticles' adhesion and crosslink [10,13,24]. Thus, in this current work, the membranes with 40% of AA could not achieve the necessary degree of PAA crosslink (i.e., low ratio of crosslinker/AA), rapidly losing the nZVI impregnated, although nZVI inside the membrane was the highest (1.27 mg/cm²). Otherwise, 20% of AA could enhance PAA crosslink (i.e., there was no iron leaching after 1 h of reaction) but lower nZVI loading.

It is important to highlight the need for preparing a stable catalytic membrane, which could enhance organic pollutant removal without losing its activity. So, considering the percentage of pollutant removal and oxidant diffusion into the membrane matrix and their contact with the impregnated nZVI on the surface and inside the pores, the membrane 30% AA* was chosen for the cross-flow experiments.

3.4. nZVI/PAA/PVDF Membrane Characterization

Membranes prepared with 30% of AA were characterized according to the techniques shown in Figure 6. The SEM image (Figure 6A) reveals agglomerated nanoparticles on the surface of the membrane. EDS (Energy Dispersive X-Ray Spectroscopy) (Figure 6C) confirms the presence of iron and suggests that it is mostly in the oxidized form. However, this could not be confirmed by X-ray Diffraction (XRD) once the PVDF polymer suppresses the signal from iron species. Nevertheless, FTIR (Figure 6B) could prove the iron loading by the shift of C=O stretches from 1718.1 to 1557.8 cm⁻¹, once nZVI is bonded to carboxyl groups from PAA [10]. FTIR spectra also present the -CF₂- bond stretching (1000–1360 cm⁻¹) without any change between the different membranes, which is characteristic of PVDF polymer [10]. The PAA crosslink could be evidenced with the appearance of C-O-C stretching vibrations in 1231.5 cm⁻¹; however, this bonding is suppressed when the nZVI is loaded [32]. C=O bond stretching related to PVP polymer is presented at 1560.7 cm⁻¹ on the PVDF membrane and shifted to 1652.3 cm⁻¹ with PAA functionalization. This is an indication that PVP has some interaction with the PAA functionalized in the surface of the membrane due to hydrogen bonds [33]. Regarding nZVI loading, the C=O stretching from PVP remained in the same wavelength (1652.3 cm⁻¹) as the PAA/PVDF membrane. The contact angle of the membranes was also measured, resulting in 43.7° for PVDF membrane and zero for PAA/PVDF and nZVI/PAA/PVDF membranes (Figure 6D). This is related to the high hydrophilicity of hydrogels features like PAA [34].

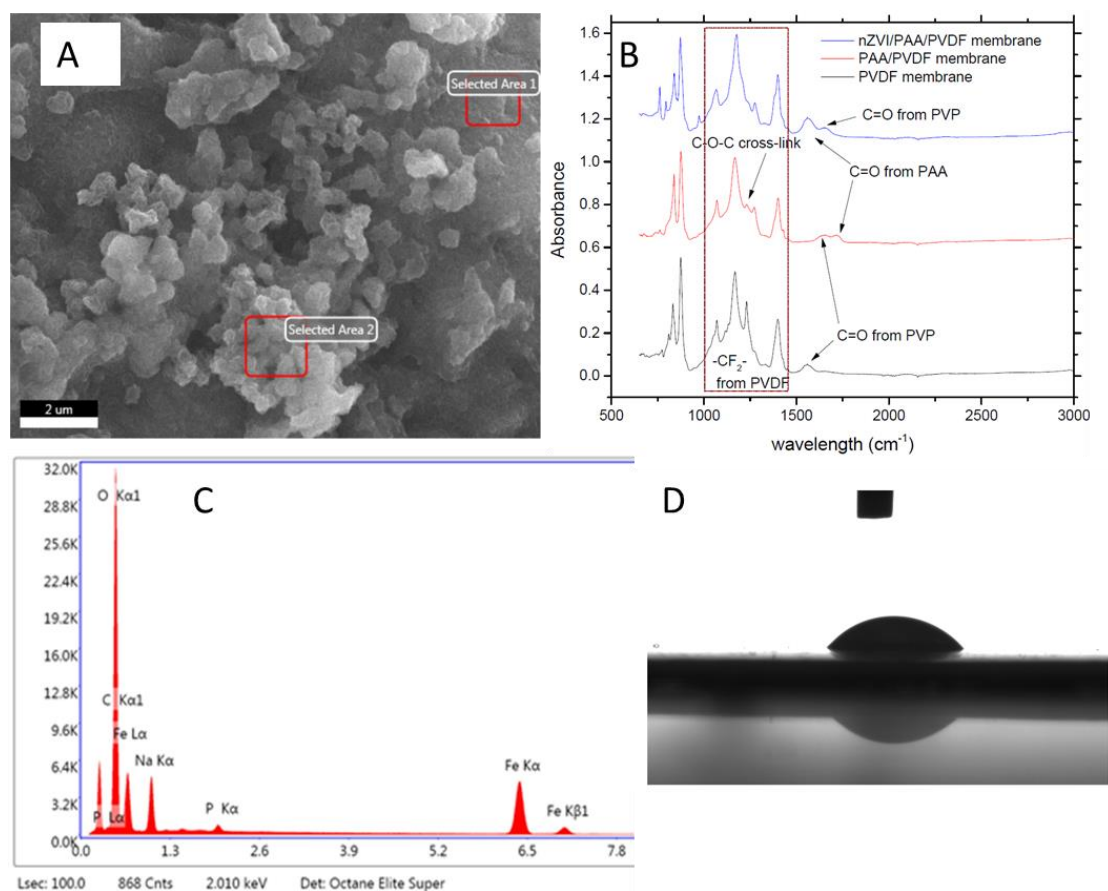


Figure 6. Membrane characterization according to: (A) nZVI membrane SEM (magnitude 10 k), (B) Fourier transform infrared spectroscopy (FTIR) of PVDF, PAA/PVDF and nZVI/PAA/PVDF membranes, (C) EDS (Energy Dispersive X-Ray Spectroscopy) of nZVI membrane, and (D) Contact angle picture of PVDF membrane. PVDF (Polyvinylidene fluoride); PAA (Polyacrylic acid).

3.5. BPA Removal in Convective Mode

To investigate the feasible application of the nZVI/PAA/PVDF membrane as well as to verify a possible improvement on BPA removal as a consequence of diffusion resistance lowering, these membranes were applied on a cross-flow system. As discussed before, nanoparticles can be a great advantage, especially when loaded in microfiltration membranes, once their major separation is driven by size-exclusion phenomena, imputing catalytic characteristics for micropollutant degradation [10,13,35].

Results from BPA removal in convective mode are shown in Figure 7A. Interaction between BPA and PVDF membranes due to adsorption phenomena [36,37] is illustrated with the reduction of BPA concentration (16%) after 3 h of permeation. When these membranes are loaded with nZVI, BPA removal presented a substantial increase, achieving 40% in 3 h, with the major activity within 30 min (33% of BPA removal). This behavior indicates the generation of $\bullet\text{OH}$ radicals by nZVI in the presence of dissolved O_2 and $\text{pH} \leq 7.0$, as discussed before [30]. It also highlights the advantage of nanoparticles loading into microfiltration membranes for organic compounds' removal. The addition of H_2O_2 to the feed solution had just a slight improvement on BPA removal (43% in 3 h). In this case, the major difference was within 15 min, where the BPA removal was 10% more than the process without H_2O_2 . As the H_2O_2 concentration increased from 0 to 20 mg/L, so the reaction of Equation (2) was dislocated to the direction of product formation, increasing $\bullet\text{OH}$ radicals' generation in the early minutes. Longer times facilitate nZVI deactivation by iron oxides depositions on the upper surface, as discussed before [10,30]. The highest BPA removal for the permeation with 20 mg/L of H_2O_2 could also be related

to the flux of these membranes (Figure 7B), which was lower ($143 \text{ L/m}^2\cdot\text{h}$ in 5 min; residence time = 10 s) than the process without oxidant addition ($295 \text{ L/m}^2\cdot\text{h}$ in 5 min; residence time = 5 s). According to Islam et al., the residence time of the target compound inside the membrane is important to enhance oxidation reactions [13]. The authors describe that by increasing it from 5 to 42 s, the dechlorination of pentachlorobiphenyl increased by almost 15% for the Pd/nZVI/PAA/PVDF membranes.

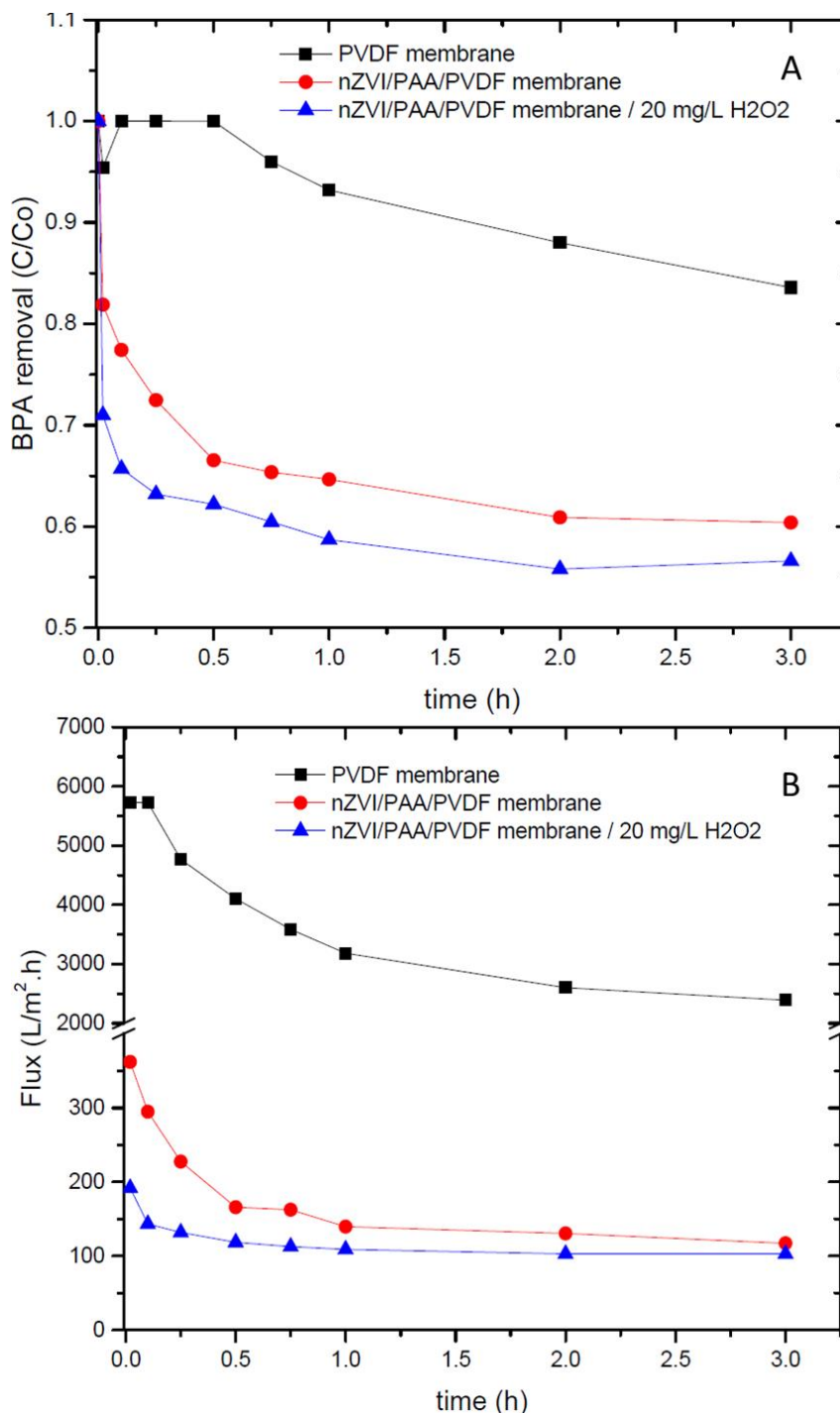


Figure 7. (A) BPA removal and (B) flux of PVDF and nZVI/PAA/PVDF membranes. Conditions: pressure 1 bar, pH 5.0, $(\text{BPA})_0 = 800 \text{ mg/L}$, and $(\text{H}_2\text{O}_2)_0 = 0$ and 20 mg/L .

Comparing the results from permeation in the cross-flow system (Figure 7A) and nZVI/PAA/PVDF membranes in solution (Figure 5A) with 1 h of reaction, the first one achieved 25% more BPA removal as

expected, once in convective mode problems with diffusion of the target compound were overcome [13]. Moreover, when the nZVI is used in solution (i.e., experimental conditions: 1 g/L of nZVI at pH 5 and 20 mg/L of BPA), 16% of BPA removal in 1 h of reaction was reported [38]. Considering the cross-flow system working in batch mode with recirculation of permeate and retentate and the total volume of feed solution with 1.5 L, nanoparticles' concentration used in this work was 0.04 mg/L. So, even though concentration in the permeation process of ZVI nanoparticles is more than 1000 times lower, BPA removal is 2 times more than the reactions with nZVI in solution. These results could be due to the turbulence intrinsic from the permeation process that enhances dissolved O₂ in the system.

4. Conclusions

nZVI/CMC in solution was evaluated for DRX-6BN and BPA removal and the results of the latter organic compound were compared with the efficiency of nZVI composite membranes in solution and the cross-flow system. Besides the high degradation rate of nZVI/CMC on the target compounds, when the nanoparticles are loaded in porous materials as PVDF membranes, their activities diminished substantially. This was confirmed according to the percentage of iron leaching from the nZVI/PAA/PVDF membranes, where a higher concentration of iron species in the bulk solution leads to enhancement of BPA removal. Problems with iron leaching were addressed by reaching the best relation of AA/EG (AA = 30% and EG = 1% mol AA) and higher nZVI loading was achieved by filtrating the AA polymeric solution through the PVDF membrane. Diffusion resistance issues were also depicted as an important parameter for porous materials, which were overcome by conducting the nZVI/PAA/PVDF membranes in a cross-flow system. Regarding the membrane separation process, nZVI poses as an important additive to microfiltration membranes, reaching 40% of BPA removal against 16% of adsorption on the neat membranes.

Author Contributions: Conceptualization, C.P.B. and F.V.F.; Data curation, L.L.S.S. and J.A.C.; Formal analysis, L.L.S.S.; Funding acquisition, C.P.B. and F.V.F.; Investigation, L.L.S.S.; Methodology, L.L.S.S.; Project administration, F.V.F.; Resources, C.P.B. and F.V.F.; Supervision, A.M.R., C.P.B. and F.V.F.; Validation, L.L.S.S.; Visualization, F.V.F.; Writing—original draft, L.L.S.S.; Writing—review & editing, A.M.R., C.P.B. and F.V.F.

Funding: This study was financed in part by the Coordenação de Aperfeiçoamento de Pessoal de Nível Superior—Brasil (CAPES)—Finance Code 001—and by Conselho Nacional de Desenvolvimento Científico e Tecnológico—Brasil (CNPq).

Conflicts of Interest: The authors declare no conflict of interest. The funders had no role in the design of the study; in the collection, analyses, or interpretation of data; in the writing of the manuscript, or in the decision to publish the results.

References

1. Son, H.S.; Im, J.K.; Zoh, K.D. Fenton-like degradation mechanism for 1,4-dioxane using zero-valent iron (Fe⁰) and UV light. *Water Res.* **2009**, *43*, 1457–1463. [[CrossRef](#)] [[PubMed](#)]
2. Kang, Y.-G.; Yoona, H.; Leeb, W.; Kimc, E.; Chang, Y. Comparative study of peroxide oxidants activated by nZVI: Removal of 1,4-Dioxane and arsenic(III) in contaminated waters. *Chem. Eng. J.* **2018**, *334*, 2511–2519. [[CrossRef](#)]
3. Bae, S.; Collins, R.N.; Waite, T.D.; Hanna, K. Advances in surface passivation of nanoscale zerovalent iron (NZVI): A critical review. *Environ. Sci. Technol.* **2018**, *52*, 12010–12025. [[CrossRef](#)] [[PubMed](#)]
4. Dong, H.; He, Q.; Zeng, G.; Tang, L.; Zhang, L.; Xie, L.; Zeng, Y.; Zhao, F. Degradation of trichloroethene by nanoscale zero-valent iron (nZVI) and nZVI activated persulfate in the absence and presence of EDTA. *Chem. Eng. J.* **2017**, *316*, 410–418. [[CrossRef](#)]
5. Guan, X.; Sun, Y.; Qin, H.; Li, J.; Lo, I.M.C.; He, D.; Dong, H. The limitations of applying zero-valent iron technology in contaminants sequestration and the corresponding countermeasures: the development in zero-valent iron technology in the last two decades (1994–2014). *Water Res.* **2015**, *75*, 224–248. [[CrossRef](#)]
6. Satapanajaru, T.; Chompuchan, C.; Suntornchot, P.; Pengthamkeerati, P. Enhancing decolorization of Reactive Black 5 and Reactive Red 198 during nano zerovalent iron treatment. *Desalination* **2011**, *266*, 218–230. [[CrossRef](#)]

7. Fu, Y.; Peng, L.; Zeng, Q.; Yang, Y.; Song, H.; Shao, J.; Liu, S.; Gu, J. High efficient removal of tetracycline from solution by degradation and flocculation with nanoscale zerovalent iron. *Chem. Eng. J.* **2015**, *270*, 631–640. [[CrossRef](#)]
8. Fu, F.; Dionysiou, D.D.; Liu, H. The use of zero-valent iron for groundwater remediation and wastewater treatment: a review. *J. Hazard. Mater.* **2014**, *267*, 194–205. [[CrossRef](#)]
9. Stefaniuk, M.; Oleszczuk, P.; Ok, Y.S. Review on nano zerovalent iron (nZVI): From synthesis to environmental applications. *Chem. Eng. J.* **2016**, *287*, 618–632. [[CrossRef](#)]
10. Gui, M.; Smuleac, V.; Ormsbee, L.E.; Sedlak, D.; Bhattacharyya, D. Iron oxide nanoparticle synthesis in aqueous and membrane systems for oxidative degradation of trichloroethylene from water. *J. Nanopart. Res.* **2012**, *14*, 861. [[CrossRef](#)]
11. Wang, Y.; Fang, Z.; Liang, B.; Tsang, E.P. Remediation of hexavalent chromium contaminated soil by stabilized nanoscale zero-valent iron prepared from steel pickling waste liquor. *Chem. Eng. J.* **2014**, *247*, 283–290. [[CrossRef](#)]
12. Osegueda, O.; Dafinov, A.; Llorca, J.; Medina, F.; Sueiras, J. Heterogeneous catalytic oxidation of phenol by in situ generated hydrogen peroxide applying novel catalytic membrane reactors. *Chem. Eng. J.* **2015**, *262*, 344–355. [[CrossRef](#)]
13. Islam, M.S.; Hernández, S.; Wan, H.; Ormsbee, L.; Bhattacharyya, D. Role of membrane pore polymerization conditions for pH responsive behavior, catalytic metal nanoparticle synthesis, and PCB degradation. *J. Membr. Sci.* **2018**, *555*, 348–361. [[CrossRef](#)] [[PubMed](#)]
14. Wang, X.; Chen, C.; Liu, H.; Ma, J. Preparation and characterization of PAA/PVDF membrane-immobilized Pd/Fe nanoparticles for dechlorination of trichloroacetic acid. *Water Res.* **2008**, *42*, 4656–4664. [[CrossRef](#)]
15. Li, X.; Sottoc, A.; Lib, J.; Van der Bruggena, B. Progress and perspectives for synthesis of sustainable antifouling composite membranes containing in situ generated nanoparticles. *J. Membr. Sci.* **2017**, *524*, 502–528. [[CrossRef](#)]
16. Pang, R.; Li, X.; Li, J.; Lu, Z.; Sun, X.; Wang, L. Preparation and characterization of ZrO₂/PES hybrid ultrafiltration membrane with uniform ZrO₂ nanoparticles. *Desalination* **2014**, *332*, 60–66. [[CrossRef](#)]
17. Pang, R.; Li, J.; Wei, K.; Sun, X.; Shen, J.; Han, W.; Wang, L. In Situ preparation of Al-containing PVDF ultrafiltration membrane via sol-gel process. *J Colloid Interface Sci.* **2011**, *364*, 373–378. [[CrossRef](#)]
18. Wang, X.; Liu, P.; Ma, J.; Liu, H. Preparation of novel composites based on hydrophilized and functionalized polyacrylonitrile membrane-immobilized NZVI for reductive transformation of metronidazole. *Appl. Surf. Sci.* **2017**, *396*, 841–850. [[CrossRef](#)]
19. Yang, J.; Wang, X.; Zhu, M.; Liu, H.; Ma, J. Investigation of PAA/PVDF-NZVI hybrids for metronidazole removal: synthesis, characterization, and reactivity characteristics. *J. Hazard. Mater.* **2014**, *264*, 269–277. [[CrossRef](#)]
20. Yang, J.; Yang, J.; Zhu, M.; Wang, X.; Alvarez, P.J.J.; Liu, K. Poly(vinylidene fluoride) membrane supported nano zero-valent iron for metronidazole removal: Influences of calcium and bicarbonate ions. *J. Taiwan Inst. Chem. Eng.* **2015**, *49*, 113–118. [[CrossRef](#)]
21. Liu, C.; Li, X.; Ma, B.; Qin, A.; He, C. Removal of water contaminants by nanoscale zero-valent iron immobilized in PAN-based oxidized membrane. *Appl. Surf. Sci.* **2014**, *321*, 158–165. [[CrossRef](#)]
22. Yanez, J.E.H.; Wang, Z.; Lege, S.; Obst, M.; Roehler, S.; Burkhardt, C.J.; Zwiener, C. Application and characterization of electroactive membranes based on carbon nanotubes and zerovalent iron nanoparticles. *Water Res.* **2017**, *108*, 78–85. [[CrossRef](#)] [[PubMed](#)]
23. Wang, X.; Wang, T.; Ma, J.; Liu, H.; Ning, P. Synthesis and characterization of a new hydrophilic boehmite-PVB/PVDF blended membrane supported nano zero-valent iron for removal of Cr(VI). *Sep. Purif. Technol.* **2018**, *205*, 74–83. [[CrossRef](#)]
24. Smuleac, V.; Bachas, L.; Bhattacharyya, D. Aqueous—Phase Synthesis of PAA in PVDF Membrane Pores for Nanoparticle Synthesis and Dichlorobiphenyl Degradation. *J. Membr. Sci.* **2010**, *346*, 310–317. [[CrossRef](#)] [[PubMed](#)]
25. Guillen, G.R.; Pan, Y.; Li, M.; Hoek, E.M.V. Preparation and Characterization of Membranes Formed by Nonsolvent Induced Phase Separation: A Review. *Ind. Eng. Chem. Res.* **2011**, *50*, 3798–3817. [[CrossRef](#)]
26. Xu, J.; Dozier, A.; Bhattacharyya, D. Synthesis of Nanoscale Bimetallic Particles in Polyelectrolyte Membrane Matrix for Reductive Transformation of Halogenated Organic Compounds. *J. Nanopart. Res.* **2005**, *7*, 449–467. [[CrossRef](#)]

27. Xu, J.; Bhattacharyya, D. Fe/Pd Nanoparticle Immobilization in Microfiltration Membrane Pores: Synthesis, Characterization, and Application in the Dechlorination of Polychlorinated Biphenyls. *Ind. Eng. Chem. Res.* **2007**, *46*, 2348–2359. [[CrossRef](#)]
28. Araujo, F.V.F.; Yokoyama, L.; Teixeira, L.A.C.; Campos, J.C. Heterogeneous fenton process using the mineral hematite for the discolouration of a reactive dye solution. *Braz. J. Chem. Eng.* **2011**, *28*, 605–6016. [[CrossRef](#)]
29. Bhatnagar, A.; Anastopoulos, I. Adsorptive removal of bisphenol A (BPA) from aqueous solution: A review. *Chemosphere* **2017**, *168*, 885–902. [[CrossRef](#)]
30. Harada, T.; Yatagai, T.; Kawase, Y. Hydroxyl radical generation linked with iron dissolution and dissolved oxygen consumption in zero-valent iron wastewater treatment process. *Chem. Eng. J.* **2016**, *303*, 611–620. [[CrossRef](#)]
31. Sharma, V.K.; Zeboril, R. Iron-based green technologies for water remediation. In *Advanced Oxidation Processes for Water Treatment*; Stefan, M.I., Ed.; IWA Publishing: London, UK, 2018.
32. Mishra, S.; Rani, G.U.; Sen, G. Microwave initiated synthesis and application of polyacrylic acid grafted carboxymethyl cellulose. *Carbohydr. Polym.* **2012**, *87*, 2255–2262. [[CrossRef](#)]
33. Chang, X.; Xanga, Z.; Quana, S.; Xu, Y.; Jianga, Z.; Shao, L. Exploring the synergetic effects of graphene oxide (GO) and polyvinylpyrrolidone (PVP) on poly(vinylidene fluoride) (PVDF) ultrafiltration membrane performance. *Appl. Surf. Sci.* **2014**, *316*, 537–548. [[CrossRef](#)]
34. Rizwan, M.; Yahya, R.; Hassan, A.; Yar, M.; Azzahari, A.D.; Selvanathan, V.; Sonsudin, F.; Abouloula, C.N. pH Sensitive Hydrogels in Drug Delivery: Brief History, Properties, Swelling, and Release Mechanism, Material Selection and Applications. *Polymers* **2017**, *9*, 137. [[CrossRef](#)] [[PubMed](#)]
35. Chen, X.; Mao, S.S. Titanium Dioxide Nanomaterials: Synthesis, Properties, Modifications, and Applications. *Chem. Rev.* **2007**, *107*, 2891–2959. [[CrossRef](#)]
36. Wang, Q.; Yang, C.; Zhang, G.; Hu, L.; Wang, P. Photocatalytic Fe-doped TiO₂/PSF composite UF membranes: Characterization and performance on BPA removal under visible-light irradiation. *Chem. Eng. J.* **2017**, *319*, 39–47. [[CrossRef](#)]
37. Escalona, I.; Grooth, J.; Font, J.; Nijmeijer, K. Removal of BPA by enzyme polymerization using NF membranes. *J. Membr. Sci.* **2014**, *468*, 192–201. [[CrossRef](#)]
38. Girit, B.; Dursun, D.; Olmez-Hanci, T.; Arslan-Alaton, I. Treatment of aqueous bisphenol A using nano-sized zero-valent iron in the presence of hydrogen peroxide and persulfate oxidants. *Water Sci. Technol.* **2015**, *71*, 1859–1868. [[CrossRef](#)]



© 2019 by the authors. Licensee MDPI, Basel, Switzerland. This article is an open access article distributed under the terms and conditions of the Creative Commons Attribution (CC BY) license (<http://creativecommons.org/licenses/by/4.0/>).